ISSN 2070-2051, Protection of Metals and Physical Chemistry of Surfaces, 2016, Vol. 52, No. 5, pp. 802–813. © Pleiades Publishing, Ltd., 2016.
Original Russian Text © A.D. Pogrebnjak, V.M. Rogoz, O.V. Bondar, N.K. Erdybaeva, S.V. Plotnikov, 2016, published in Fizikokhimiya Poverkhnosti i Zashchita Materialov, 2016, Vol. 52, No. 5, pp. 488–499.

NANOSCALE AND NANOSTRUCTURED MATERIALS AND COATINGS

# Structure and Physicomechanical Properties of NbN-Based Protective Nanocomposite Coatings: A Review

**A. D. Pogrebnjak[a, b, *], V. M. Rogoz[a, c], O. V. Bondar[a, c], N. K. Erdybaeva[d], and S. V. Plotnikov[d]**

[a] *Department of Nanoelectronics, Sumy State University, ul. Rimskogo-Korsakova 2, Sumy, 40007 Ukraine*
[b] *Lublin University of Technology, Lublin, 20-618 Poland*
[c] *NBMC, Adam Mickiewicz University of Poznan, Poznan, Poland*
[d] *East Kazakhstan State Technical University, Ust-Kamenogorsk, Kazakhstan*
**e-mail: alexp@i.ua*

Received October 17, 2015

**Abstract**—This review summarizes the present-day achievements in the study of the structure and properties of protective nanocomposite coatings based on NbN, NbAlN, and NbSiN prepared by a variety of modern deposition techniques. It is shown that a change in deposition parameters has a significant effect on the phase composition of the coatings. Depending on the magnitude of negative potential on the substrate, the pressure of nitrogen or a nitrogen–argon mixture in the chamber, and the substrate temperature, it is possible to obtain coatings containing different phases, such as NbN and $SiN_x$ ($Si_3N_4$), AlN, and $NbAl_2N$. It is found that, in the case of formation of the ε-NbN phase, the coatings become very hard; their hardness achieves values on the order of 53 GPa. At the same time, they remain thermally stable at temperatures of up to 600°C, chemically inert, and resistant to wear. The effect of the nanograin size, the volume fraction of boundaries and interfaces, and the point defect concentration on the physicomechanical properties of these coatings is described. Niobium nitride-based coatings can be used in superconducting systems and single-photon detectors; they are capable of operating under the action of strong magnetic fields of up to 20 T; they can be used in integrated logic circuits and applied as protective coatings of machine parts, edges of cutting tools, etc.

**DOI:** 10.1134/S2070205116050191

## INTRODUCTION

Niobium nitride (NbN) has a high transition temperature and is classified as a refractory compound; these features make it promising for practical applications [1]. A potential application of niobium nitrides in engineering is in the design of devices based on a superconductor–insulator–superconductor (SIS) junction. Superconducting devices with SIS junctions are prepared from materials based on Pb, Nb, and NbN [2, 3–14]. NbN-based coatings are used in the design of large-scale Josephson integrated logic circuits [15–18], bolometers [19–24], and superconducting single-photon detectors [25–30]. An advantage of NbN coatings is the preservation of the characteristics of the device in a wide temperature range of 4–300 K. In addition, since NbN-based coatings are capable of operating under the action of strong magnetic fields of up to 20 T at a current density of up to 4000 A/cm$^2$, these coatings are a high-priority material for use in devices operating under the action of high-intensity electromagnetic fields [31–35].

Deposition of niobium nitrides is a more complex process than the deposition of pure Nb because the superconducting phase of NbN is metastable [7] and the coating should be deposited by reactive sputtering. It is known that optimization and control of reactive ion sputtering are fairly complicated [36–38] because of the hysteresis effect that occurs upon the addition of a reactive gas that affects the coating stoichiometry directly during deposition. Nb–X–N coating is mostly deposited via chemical vapor deposition (CVD) [39, 40] or physical vapor deposition (PVD) techniques [41–52]. Coating deposition parameters, such as the substrate temperature, the flow rate, the energy of atoms and ions incident on the surface of the growing coating, and the deposition rate, have a significant effect on the chemical composition and structure of the coating. It was found that it is necessary to provide a high substrate temperature [53, 54] or introduce impurities [8, 55–60] to obtain a superconducting phase of NbN with a critical temperature of about 16 K. The main feature of the currently available magnetron sputtering method [9–11] is the possibility of depositing coatings without introducing impurities or heating the substrate to high temperatures.

To explore the possibility of improving the functional properties of NbN-based coatings, nanocrystalline and amorphous ternary systems, such as Nb–Al–N, Nb–Si–N, and other Nb–X–N systems, were studied

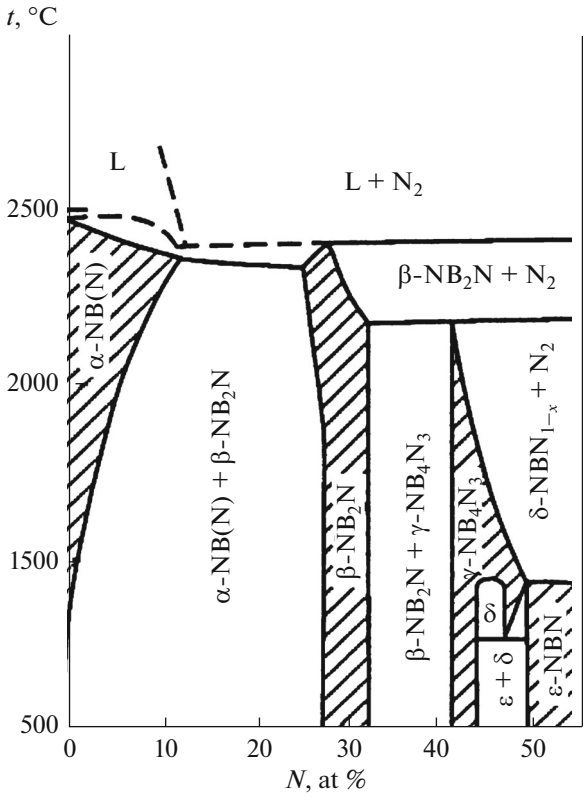


**Fig. 1.** Equilibrium phase diagram of NbN [1].

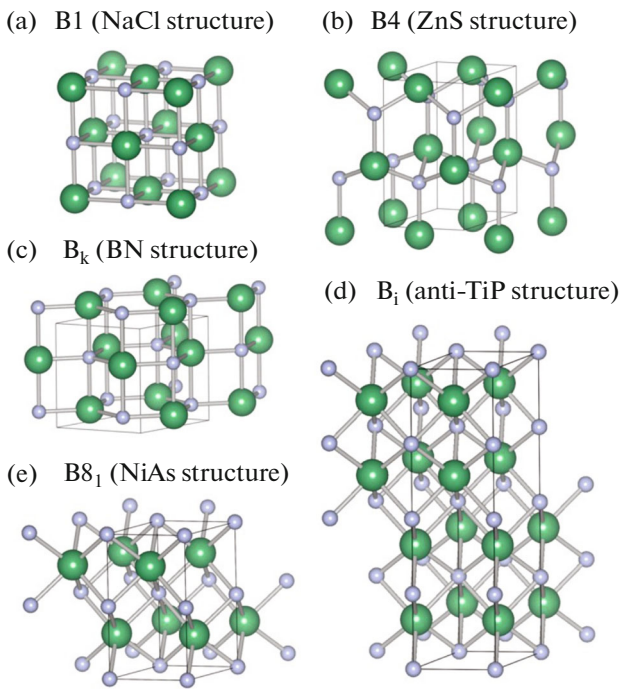


**Fig. 2.** Crystallographic structures of NbN and Nb–Al–N: (a) cubic B1, (b) wurtzite B4, (c) hexagonal $B_k$, (d) hexagonal $B_i$, and (e) hexagonal $B8_1$. Small blue and large green spheres indicate nitrogen and metal atoms, respectively [85].

[39–80]. The studies revealed that the addition of Al or Si in binary NbN compounds leads to a significant improvement of the hardness, thermal stability, and chemical inertness of the coatings [41–45]. In particular, it was shown that Nb–Si–N coatings can be used as diffusion barriers and electrodes for phase-change random-access memory devices. The addition of silicon provides the formation of a solid solution of a single-phase $Nb_{1-x}Si_xN$ material or a nanocomposite (amorphous $SiN_x$ and NbN nanocrystallites). The physical and mechanical properties of coatings are significantly affected by the grain size, grain surface, intergrain regions, and point defect density. It should be noted that the sizes of crystals in these nanocomposite coatings are as small as a few nanometers. The location and chemical composition of the amorphous $SiN_x$ phase has a dominant effect on the electrical and mechanical properties of the coating [60–63].

In view of the extensiveness of the issue of properties of NbN-based coatings, this review is limited to the problems of structure formation and improvement of the protective properties of niobium nitride-based nanocomposite coatings depending on deposition parameters.

## CRYSTAL STRUCTURE AND MORPHOLOGY OF NbN-BASED COATINGS

According to the phase diagram for NbN (Fig. 1), for deposition at room temperature and a nitrogen concentration above 45%, two different phases can be identified in the coating, namely, δ-NbN with a cubic B1 structure (Fig 2a, NaCl, #225, *Fm*3*m*), which is described in detail in [81–84] and ε-NbN with a hexagonal $B_i$ structure (Fig. 2d, TiP, #194, $P6_3/mmc$) [81, 83]. A specific feature of thin coatings is the presence of δ'-NbN with a hexagonal $B8_1$ structure (Fig. 2e, NiAs, #194, $P6_3/mmc$) [82, 84].

In the case of addition of aluminum, the Al–N compound has the form of a wurtzite B4 phase (Fig. 2b, ZnS, #186, $P6_3/mc$) [2]. In addition, the hexagonal $B_k$ structure (Fig. 2c, BN, #194, $P6_3/mmc$) is taken into account because it is similar to the B1 and B4 structures and can act as an intermediate in the transition from the B1 to B4 structure.

The authors of [86] studied the structural phase state, nanograin properties and sizes, and hardness and microstrains of NbN and Nb–Si–N nanocomposite coatings prepared by magnetron sputtering under different deposition conditions. The experimental results for the deposited Nb–Si–N films were explained on the basis of data of first-principle molec-

ular dynamics calculations of $NbN/Si_xN_y$ heterostructures.

Figure 3 shows the atomic configurations of δ-$Si_3N_4$(001) heterostructures. It is evident that the optimization of the initial heterostructure geometry at 0 K has preserved the heteroepitaxial structure, as described for the $TiN(001)/Si_3N_4$ heterostructure. At 1400 K, the δ-$Si_3N_4$(001) interface structure undergoes changes. The nitrogen atoms undergo almost symmetrical "downward" and "upward" shifts in the layers above and below the boundary layer, the silicon atoms are also shifted, and about half the Si–N bonds are broken. These events lead to the formation of distorted $Si_3N_4$-like blocks, which are represented by individual $SiN_4$ and $SiN_5$ clusters. The high-temperature (HT) heterostructure comprises, along with new $Si_3N_4$-like blocks, initial B1–$SiN_6$ clusters.

Since the length of the Si–N bond in β-$Si_3N_4$ (1.75–1.77 Å) is much shorter than the length of the Nb–N bonds in pure NbN (2.205 Å), the $NbN/Si_xN_y$ interfaces experience stresses. These stresses and the tendency of silicon to form a fourfold coordination with nitrogen atoms (as in $Si_3N_4$) are the main factors that cause changes in the interface layers. Comparison of the structure and structural functions of the HT δ-$Si_3N_4$(001) interface with the parameters calculated in [28] for amorphous $Si_3N_4$ shows that the interface structure is very similar to the structure of supercoordinated amorphous $Si_3N_4$. Thus, the structure of the HT δ-$Si_3N_4$(001) interface is amorphous, rather than heteroepitaxial; this finding is consistent with experiments of [86].

Figure 4 shows the HT hexagonal ε-$NbN(001)/Si_xN_y$ and δ-$NbN(111)/Si_xN_y$ heterostructures. Analysis of the atomic configurations and total energies of zero-temperature (ZT) and HT heterostructures shows that ε-SiN(001), ε-$Si_3N_4$–$Si_2N_3$(001), and δ-SiN(111) heterostructures vary only slightly with temperature. The initial heteroepitaxial layer in the ε-SiN(001) heterostructure undergoes changes even during static relaxation at 0 K. The interfaces in the ε-$Si_3N_4$–SiN(001) and δ-$Si_3N_4$–$Si_2N_3$(111) heterostructures become amorphous at a high temperature. As a consequence, the total energy of these systems increases with temperature.

Finally, an increase in the temperature of the δ-$Si_3N_4$–SiN(111) heterostructure contributes to the optimization thereof and a decrease in the total energy. The fourfold coordination of the silicon atoms in the $Si_3N_4$–SiN and $Si_3N_4$–$Si_2N_3$ interfaces is preserved at high temperatures. It is evident that, in the δ-SiN(111) heterostructure, the interface is heteroepitaxial and temperature-independent. These results show that, of all the discussed possible configurations of interfaces, only the HT ε-$Si_3N_4$–$Si_2N_3$(001), δ-SiN(111), and δ-$Si_3N_4$– SiN(111) interfaces are ordered.

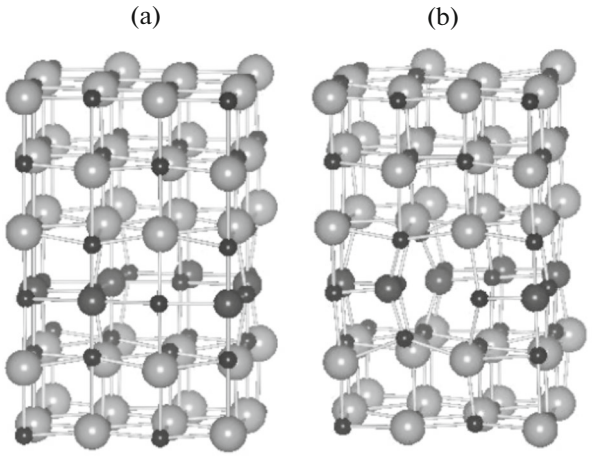


**Fig. 3.** Atomic configurations of the $NbN(001)/Si_{0.75}N$ heterostructures: (a) ZT in equilibrium and (b) HT in equilibrium. Bond length cutoff: (Si–N) 2.3 Å and (Nb–N) 2.6 Å. Gray spheres denote Nb atoms; large and small black spheres stand for Si and N atoms, respectively [86].

Results of first-principle calculations of $NbN/Si_xN_y$ heterostructures show that, in the absence of lattice defects, the formation of the $Si_xN_y$ interface does not lead to the strengthening of chemical bonds and an increase in the ideal tensile strength of the nanocomposites.

Data of experimental and theoretical studies of Nb–Al–N coatings prepared by magnetron sputtering in an Ar–$N_2$ atmosphere under different deposition conditions are described in [87]. Experimental results of the studies of the structure of Nb–Al–N coatings were also verified using first-principle calculations of B1–NbN, B1–$Nb_xAl_{1-x}N$ solid solutions, the B1–NbN(001)/B1–AlN heterostructure, and the ordered $Nb_2AlN$ phase. For calculations, the authors used 96-atomic structures constructed via translating the 8-atomic B1–NbN cell to form a 2 × 2 × 3 cell and selected identical compositions of solid solutions and heterostructures. The studied structures include all the possible configurations of the $Nb_xAl_{1-x}N$ system.

Figure 5 shows the atomic configurations of the B1–NbN(001)/1 ML AlN and B1–NbN(001)/2 ML B1–AlN heterostructures, the ML-monolayer, and B1–$Nb_xAl_{1-x}N$ solid solutions. Analysis of the total energies of the heterostructures and the solid solutions shows that B1–$Nb_xAl_{1-x}N$ solid solutions for $x < 0.67$ should undergo decomposition; at these concentrations, a nanocomposite structure composed of B1–NbN and B1–AlN crystallites can be formed. The atomic configurations determined by first-principle calculations were used to calculate X-ray diffraction patterns for the B1–NbN(001)/2 ML B1–AlN heterostructure and the B1–NbN, B1–$Nb_xAl_{1-x}N$ ($x \sim 0.67$), and $Nb_2AlN$ phases. The calculated XRD spec-

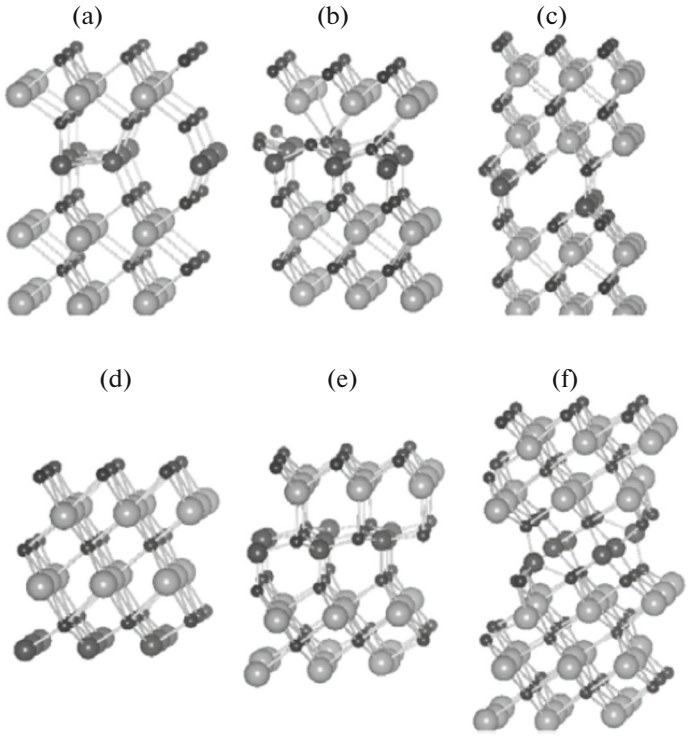


**Fig. 4.** Atomic configurations of the HT heterostructures: (a) ε-SiN(001), (b) ε-$Si_3N_4$–SiN(001), (c) ε-$Si_3N_4$–$Si_2N_3$(001), (d) δ-SiN(111), (e) δ-$Si_3N_4$–SiN(111), and (f) δ-$Si_3N_4$–$Si_2N_3$(111). Bond length cutoff: (Si–N) 2.3 Å and (Nb–N) 2.6 Å. Designation of atoms is the same as in Fig. 3 [86].

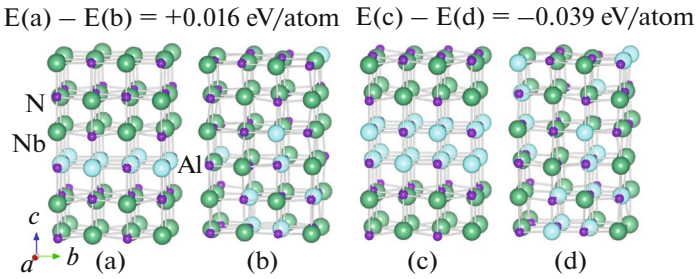


**Fig. 5.** Atomic configurations of (a) the B1–NbN(001)/1 ML B1–AlN heterostructure, (b) the $Nb_{0.83}Al_{0.17}N$ solid solution, (c) the B1–NbN(001)/2 ML B1–AlN heterostructure, and (d) the $Nb_{0.67}Al_{0.33}N$ solid solution. The composition of structures (a) and (b) is the same; accordingly, the composition of heterostructure (c) is identical to the composition of solid solution (d). The inscription above the figure represents the difference between the total energies of the heterostructure and the respective solid solution with a random arrangement of atoms in the metal lattice [87].

tra are shown in Fig. 6. In comparing the results of theoretical and experimental studies, the authors have speculated that the films do not contain either $Nb_2AlN$ or B1–AlN crystallites and contain aluminum nitride in the form of an amorphous phase. The theoretical results show that the films are composed of B1–NbN and B1–$Nb_xAl_{1-x}N$ ($x \sim 0.67$) crystallites incorporated into an amorphous a-AlN matrix. This conclusion is supported by the fact that, for each of the (200) and (400) diffraction peaks, the difference between the peak positions $\Delta 2\Theta = 2\Theta(B1–NbN) – 2\Theta(B1–Nb_xAl_{1-x}N)$ in the experimental and theoretical diffraction patterns is almost the same. Niobium nitride-based films are prone to accumulating small amounts of oxygen, which can replace a portion of nitrogen in the solid solutions and the amorphous matrix. Therefore, for the solid solutions and the amorphous matrix, a more realistic structure is $Nb_xAl_{1-x}N_yO_{1-y}$, where $x \sim 0.67$ and $1 - y << 1$, and a-AlNO, respectively.

For NbN coatings prepared by magnetron sputtering, the effect of pressure [88] and substrate bias [89] on the phase composition of the coating was studied

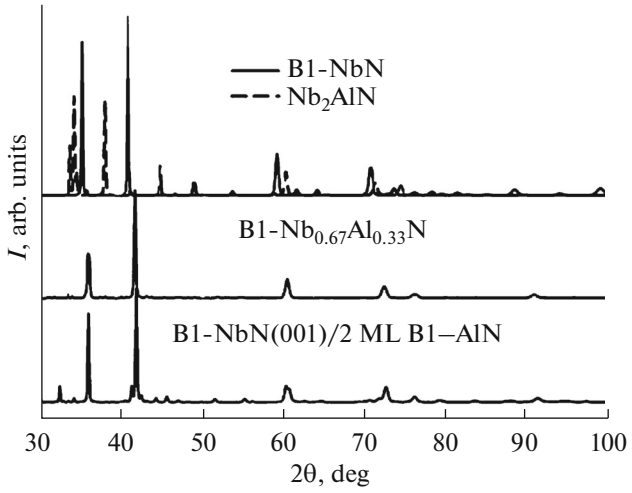


**Fig. 6.** Calculated X-ray diffraction patterns for the Nb–Al–N coatings [87].

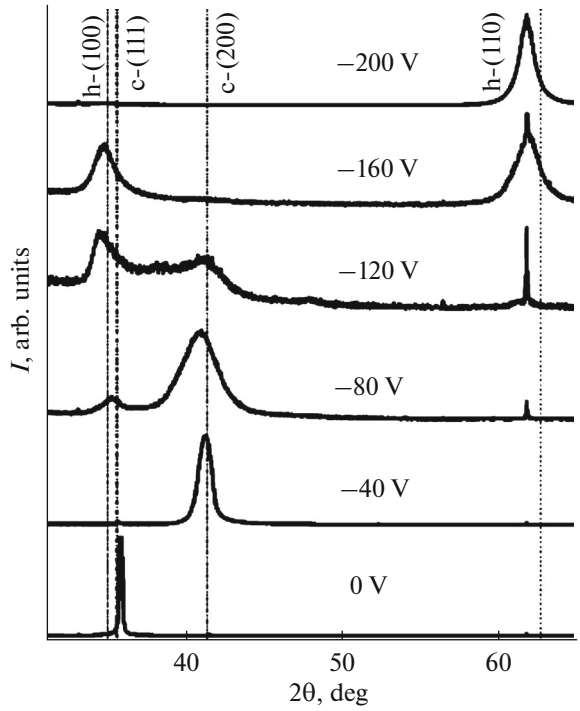


**Fig. 7.** Phase composition as a function of substrate bias for the NbN coating [89].

by XRD (Figs. 7, 8). At low nitrogen concentrations ($x = 0.57$ and 0.64), the β-$Nb_2N$ phase with a hexagonal structure is observed; in the phase diagram shown in Fig. 1, this phase corresponds to regions with a nitrogen concentration of 36.3 and 39%, respectively, However, unlike the bulk samples, the δ-NbN phase appears at a nitrogen concentration of 39%. At concentrations above 47.9%, the phase composition undergoes transformation into δ- and δ'-NbN.

It should be noted that the application of a zero bias potential to the substrate during coating deposition leads to the formation of a δ-NbN texture with the preferred (111) orientation; in the case of application of a potential of –40 to –80 V, the growth direction changes to (200). At –80 V, the (111) phase appears; an increase in the substrate bias above –120 V leads to the formation of the δ'-NbN(100) phase. With an increase in the bias to –160 V, only the δ'-NbN(100) and δ'-NbN(110) phases remain. With a further increase in the bias potential, only the (110) phase is observed in the coating.

The authors of [90] speculated that grain growth in thin coatings is provided by minimization of the strain energy and surface energy of the coating. Hence, the ratio of these two energies has an effect on the coating structure. It is shown in [91] that the surface energy of δ-NbN(200) is low; therefore, low voltages should provide the formation of a structure with the (200) texture orientation; in this case, the surface energy makes the main contribution to the total energy of the system. The application of a high bias potential to the substrate during coating deposition leads to the occurrence of a preferred orientation with the dominant elastic strain energy, which corresponds to the δ-NbN(111) phase. The strain energy of the δ'-NbN(100) and δ'-NbN(110) phases is lower than that of δ-NbN(111). Thus, it is reasonable to expect that the texture of δ'-NbN is formed owing to the minimization of the strain energy; hence, a pure δ'-NbN phase takes place only at a high compressive stress.

The studies of the phase composition of Nb–Si–N coating as a function of silicon concentration (Fig. 9) showed that, in the absence of Si, two phases—δ and δ'—are observed. At a Si concentration of 1.1–10.7 at %, only the δ phase is detected. At a Si concentration above 10.7 at %, the coating becomes amorphous.

All the Nb–Si–N coatings have the [200] growth direction, except for those containing 3.2 at % Si (the [111] growth direction) and 4.9 at % Si (no particular growth direction). Coatings of pure NbN have a grain size of about 5 nm. At a silicon concentration of 1.1 at %, the grain size increases to 12 nm; this finding is attributed to the transformation of the two-phase (δ and δ') structure into a single-phase (δ) structure. With an increase in the silicon concentration to 4.9 at %, the grain size remains unchanged; at a value of 6.5 at %, the grain size increases to 18 nm. Silicon nitride was not detected during the studies; this fact suggests the presence of this material in an amorphous state.

In the study of the dependences of the phase composition of the coatings on the substrate bias (Fig. 10), the presence of the δ-NbN(200) phase at $U_s = -50$ V can be observed. An increase in the bias to $U_s = -100$ V leads to a decrease in the δ-NbN(200) peak and the formation of δ-NbN(111) (this finding may also be associated with a decrease in the Si concentration with increasing bias potential). An increase in the bias

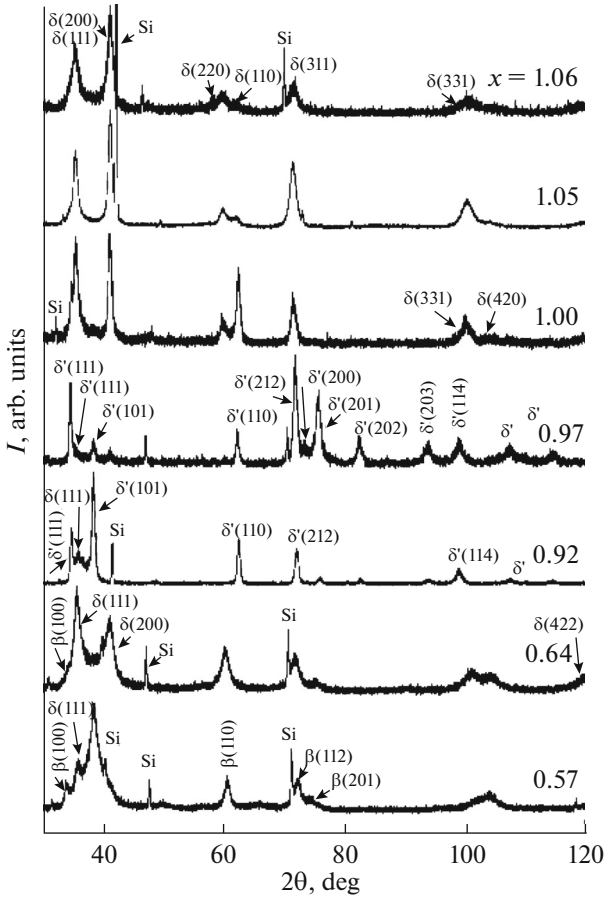


**Fig. 8.** X-ray diffraction patterns of the $NbN_x$ coating at a substrate temperature during deposition of 400°C and varying $P_{N2}$ and $x$ = N/Nb ratio [89].

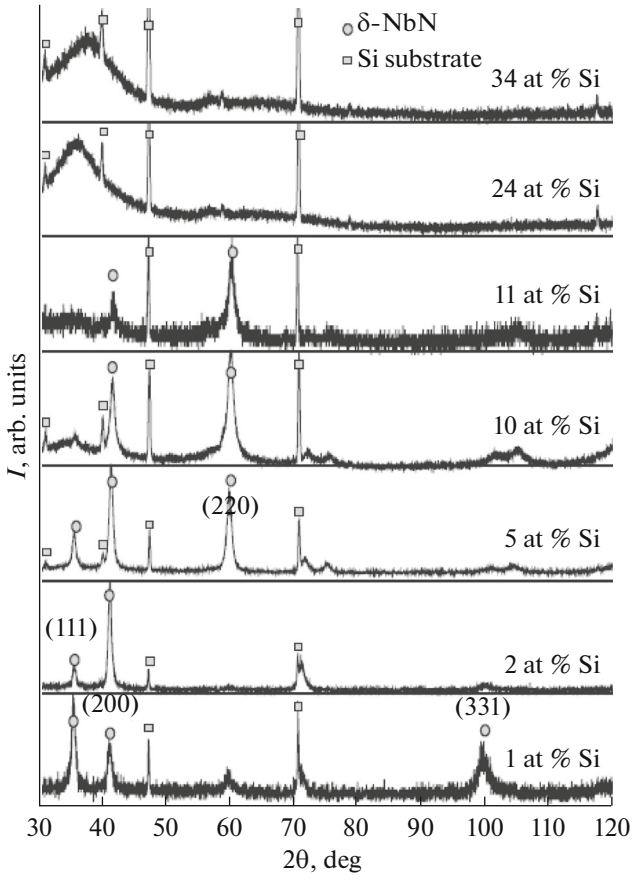


**Fig. 9.** X-ray diffraction patterns of the Nb–Si–N coating at varying Si concentration [92].

potential to $U_s = -100$ V leads to the disappearance of the δ-NbN(200) peak and the formation of hexagonal ε-NbN(004) and ε-NbN(110) phases; these features are characteristic of NbN coatings at an increase in the nitrogen pressure in the chamber to 0.04 Pa during deposition [95]. The authors of [93] argue that the formation of ε-NbN phases is attributed to a high degree of nitriding of Nb, as confirmed by the phase diagram in Fig. 1.

## SEM AND TEM STUDIES OF NbN-BASED COATINGS

At low substrate potentials during the deposition of NbN coatings (Fig. 11) [96], a columnar structure is not observed. An increase in the bias potential to –150 V leads to the formation of a coarse columnar structure. The best structure is observed at a bias potential of –200 V; a further increase in the substrate bias leads to a deterioration of the quality of the structure, which is associated with the kinetic energy of the argon and niobium ions, which affect the surface quality. Extremely high energy bias potentials (higher than –200 V) lead to collapse of the structure; low values (up to –150 V) are not sufficient for effective structure formation.

For Nb–Si–N coatings at low concentrations (up to $C_{Si}$ = 4.9 at %), a columnar structure is observed (Fig. 12) [97]. At a Si concentration of more than 12 at %, a common structure is still present in the coating, although crystallites of different orientations are formed within each of the columns; as a consequence, excess stress is eliminated. The columnar structure disappears at a silicon concentration of 24 at %.

At a silicon concentration of 20 at %, the coating is a mixture of well-crystallized columns located inside a quasi-amorphous matrix. A XEDS study shows that the silicon content in the crystallite and the quasi-amorphous matrix is 23 and 18 at %, respectively (Fig. 13).

## ELECTRONIC STRUCTURE OF NbN-BASED COATINGS

In coatings with a silicon concentration of up to 1.1 at % (Fig. 14), a binding energy peak at 99.4 eV is observed. Another binding energy peak at 101.2 eV appears with increasing silicon concentration and

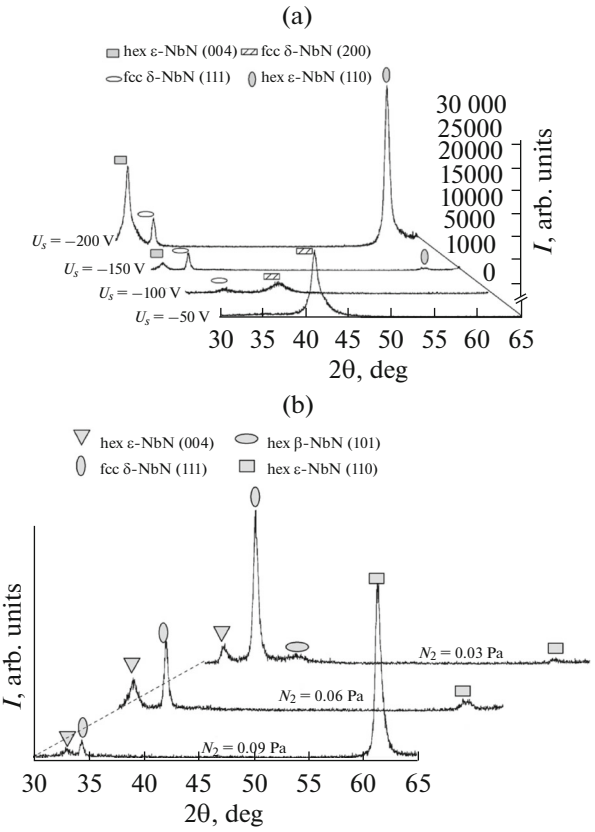


**Fig. 10.** X-ray diffraction patterns of the Nb–Si–N coating (a) at varying substrate bias potential $U_s$ [93] and (b) at varying nitrogen pressure $P_{N2}$ [94].

becomes pronounced at a value of 6.5 at %. This peak corresponds to the transformation of free Si into $Si_3N_4$ and the replacement of the Si–Si bonds by Si–N.

## OXIDATION PROCESSES IN NbN-BASED COATINGS

The authors of [98] (Fig. 15) conducted XPS studies of the stoichiometry of NbN coatings after long-term oxidation at room temperature (300 K). Simulation of the Nb 3*d*, N 1*s*, and O 1*s* peaks shows that NbN coatings are characterized by the formation of the following oxides:

(a) dielectric $Nb_2O_5$, which is the most stable form of the oxide coating;

(b) dielectric $Nb_2N_{2-x}O_{3+x}$ ($x \leqslant 1$);

(c) NbNO and $NbO_2$, which form defects at the boundary with metal compounds; and

(d) $NbN_{1-x}O_x$ ($x \approx 0.2$) and NbO, which form a layer on the metal surface.

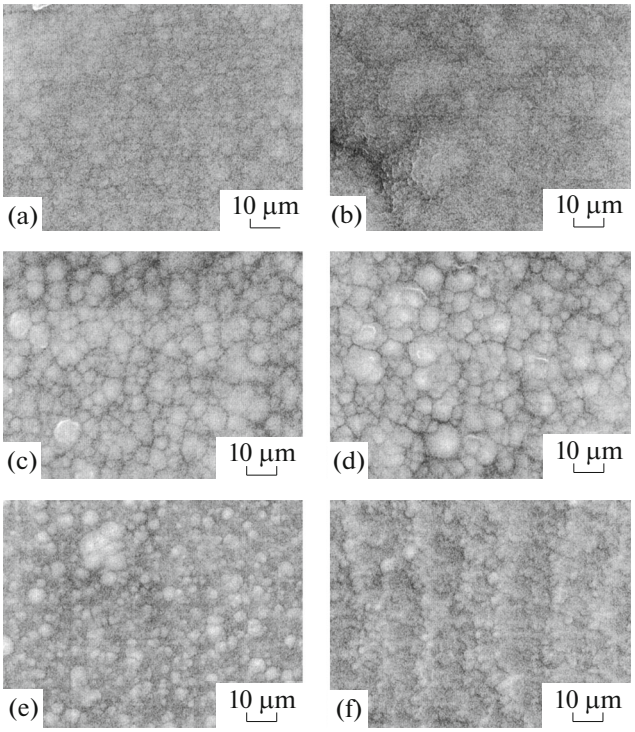


**Fig. 11.** SEM micrographs of the NbN coating at different deposition potentials: (a) 0, (b) −50, (c) −100, (d) −150, (e) −200, and (f) −250 V [96].

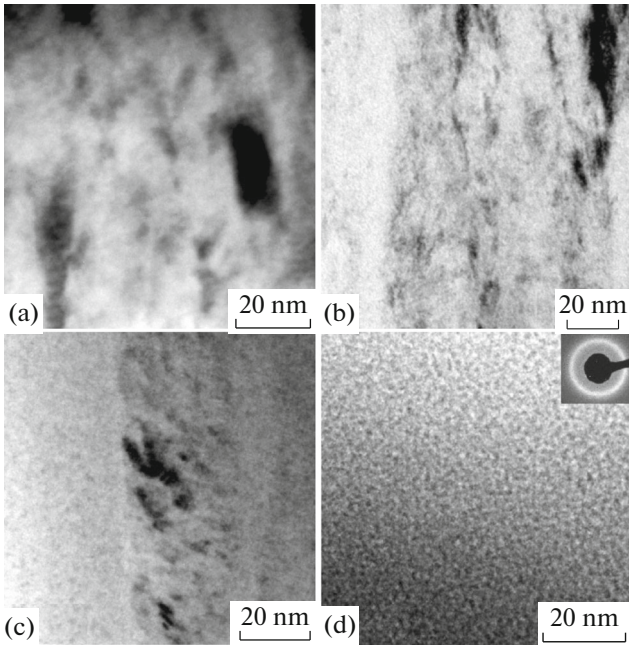


**Fig. 12.** TEM images of the Nb–Si–N coating with varying Si concentration: $C_{Si}$ = (a) 4.9, (b) 12.7, (c) 20.0, and (d) 24.0 at % [97].

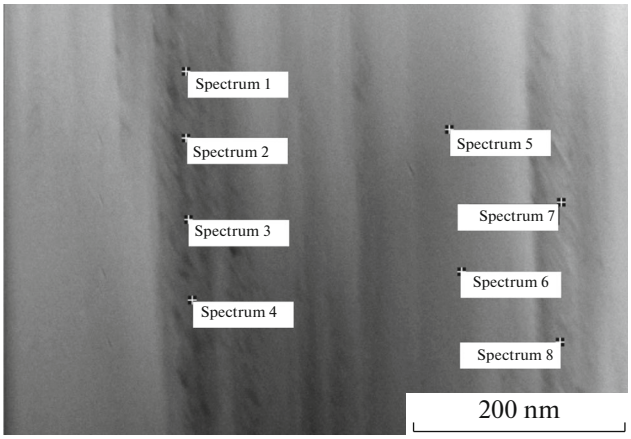


**Fig. 13.** STEM image with marked points for XEDS analysis in the Nb–Si–N coating with a silicon concentration of 20 at %.

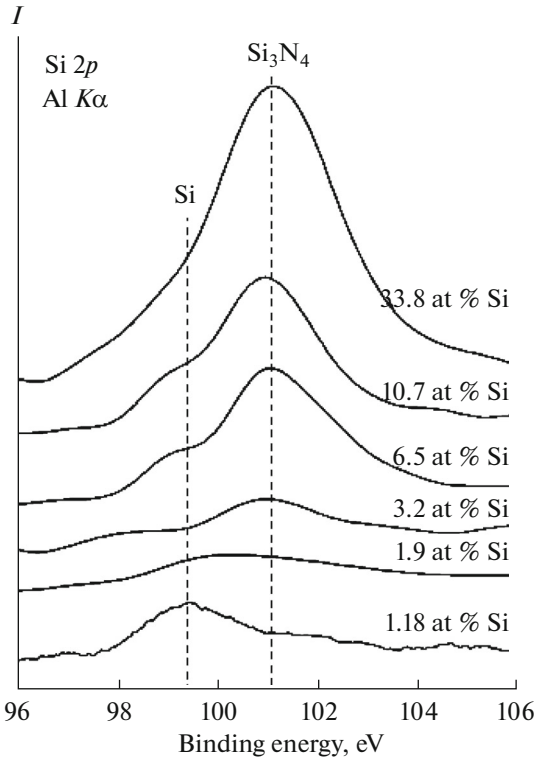


**Fig. 14.** Si 2*p* XPS spectra in the Nb–Si–N coating with varying Si concentration [92].

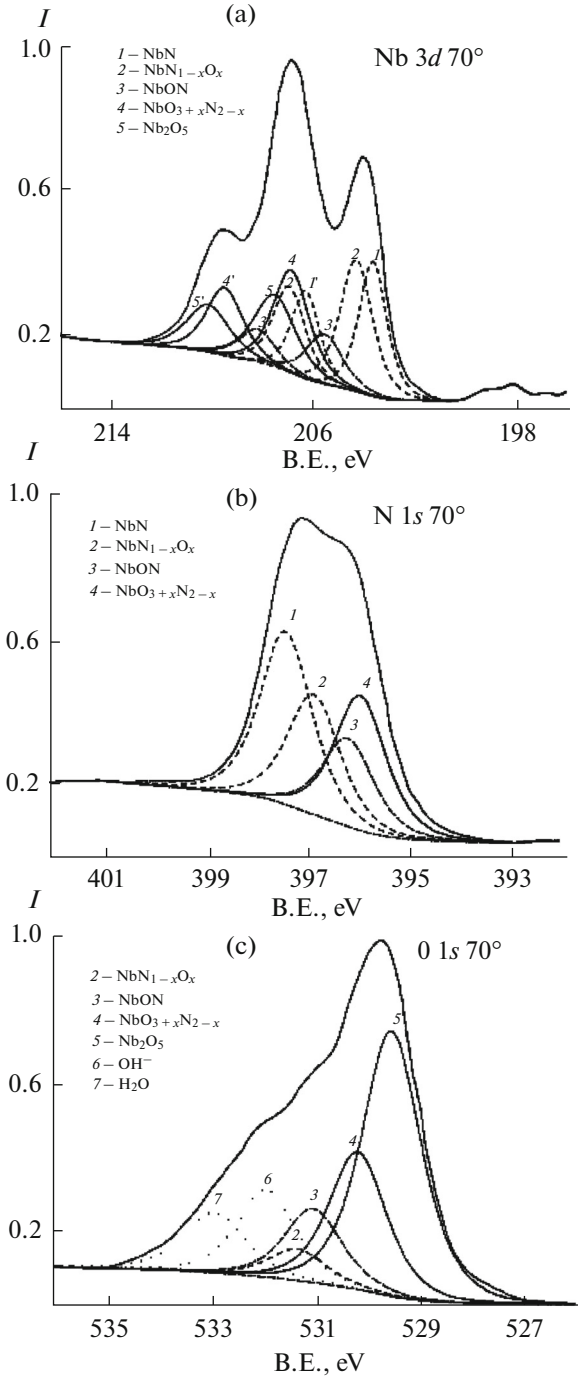


**Fig. 15.** XPS spectra of NbN coatings after oxidation: (a) the Nb 3*d*, (b) N 1*s*, and (c) O 1*s* spectrum lines [97].

## MECHANICAL PROPERTIES OF NbN-BASED COATINGS

It is known that the dominant phase in the coating has a significant effect on the mechanical properties of the coating (Fig. 16) [99]. Coatings with a dominant ε-NbN phase exhibit the highest hardness; this feature is attributed to a more intense ion bombardment at high bias potentials. Thus, in the coatings deposited at a substrate bias potential of –50 and –100 V, the dominant formation of a ε-NbN phase is observed; this factor provides nanohardness values of 45 and 41 GPa, respectively. At the same time, the coatings with dominant β-$Nb_2N$ and δ-NbN phases exhibit a nanohardness and a Young's modulus of 30 and 300 GPa, respectively.

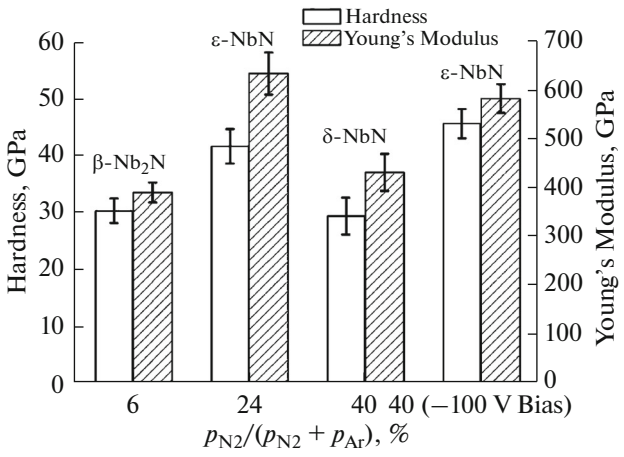


**Fig. 16.** Hardness and Young's modulus of $NbN_x$ coatings deposited at varying pressure and bias potential [99].

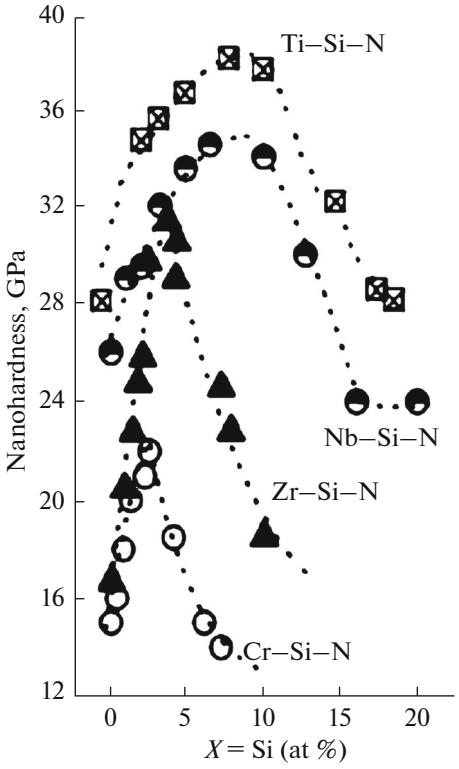


**Fig. 17.** Nanohardness as a function of Si concentration in Me–Si–N coatings (Me = Ti, Nb, Zr, Cr) [97].

Similar dependences of nanohardness on silicon concentration are observed for all Me–Si–N coatings (Fig. 17). These structures obey two basic mechanisms of formation of a high coating hardness—the formation of a hard alloy of Si atoms in the Me–N lattice or the formation of an nc-Me–N nanocomposite and an amorphous phase comprising silicon atoms. Internal stresses do not have a substantial effect on hardness [100].

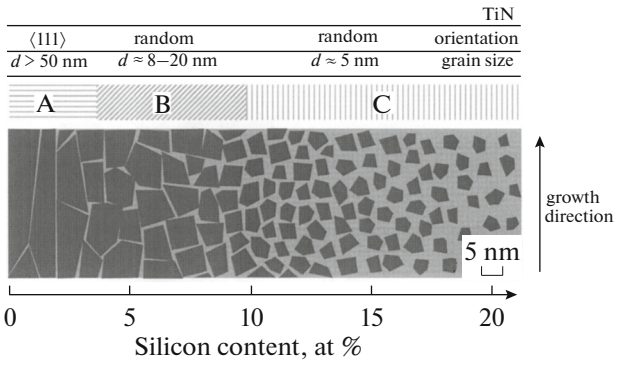


**Fig. 18.** Model of morphological zones for the nc-TiN/a-$Si_3N_4$ coating. The dark and light regions denote the nanocrystalline and amorphous coating, respectively [101].

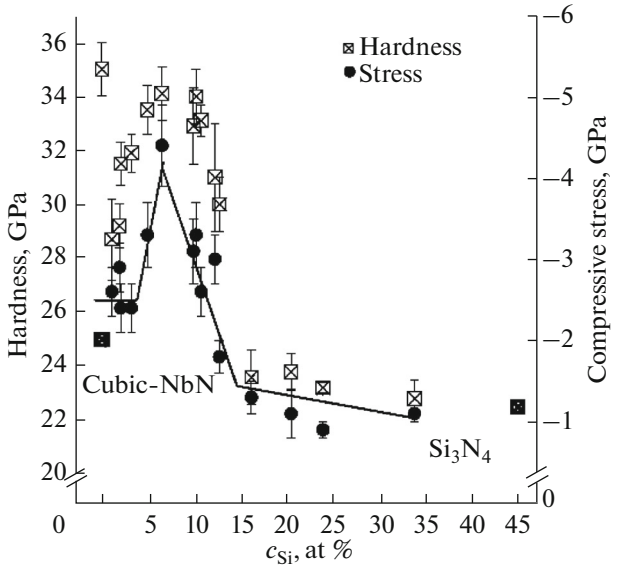


**Fig. 19.** Nanohardness and compressive stresses as a function of Si concentration in the Nb–Si–N coating.

Morphological zones as a function of silicon concentration are shown in Fig. 18 [101]. It is evident that, at a low silica content, the coating is characterized by the presence of large elongated grains in zone A, the complete interpenetration of the two phases in zone B, and the presence of isolated nanocrystals in zone C.

Hardness measurements in pure NbN showed a nanohardness at a level of 35 GPa (Fig. 19). This high hardness is provided by the δ' phase with a hardness of 40 GPa. The addition of Si leads to an abrupt decrease in the coating hardness to 25 GPa owing to the presence only of the cubic δ-phase. As the silicon concentration increases from 1.1 to 4.9 at %, the nanohardness increases to 34 GPa because the silicon atoms form a solid solution in the NbN lattice. At a silicon concentration of 4.9–11.0 at %, the coating exhibits a

stable nanohardness at a level of 34 GPa; this feature indicates the formation of a nanocomposite coating. At a higher silicon concentration, the nanohardness decreases owing to a decrease in the nanocrystal sizes and an increase in the amorphous component [97]. It should be noted that this behavior of the dependence of nanohardness is characteristic of compounds of the Me–Si–N type.

Compressive stresses, which are generated owing to the difference in the thermal expansion of the substrate and the coating, are about 0.4 GPa. At silicon concentrations of up to 3.2 at %, no changes in the compressive stress are observed. An increase in the silicon concentration to 6.5% leads to an increase in the stresses; however, with a further increase in the silicon concentration, the compressive stress decreases again. Compressive stress variations as a function of concentration suggest that the coating undergoes microstructural changes.

## CONCLUSIONS

The main results of studies of niobium nitride-based coatings—NbN, Nb–Al–N, and Nb–Si–N—prepared by a variety of modern deposition techniques have been briefly reviewed. Particular attention has been paid to the structure and physicomechanical properties of the coatings. It has been shown that the deposition parameters and the addition of silicon or aluminum in varying proportions have a significant effect on the coating structure, phase composition, hardness, and Young's modulus; in some cases, the two last-mentioned parameters can achieve values of up to 45 and 300 GPa, respectively. These mechanical properties make the discussed coatings promising for use as protective coatings for machine parts and edges of cutting tools.

## REFERENCES


1. Holleck, H., *Binäre und ternäre Carbide und Nitride der Übergangsmetalle und ihre Phasenbeziehungen,* Karlsruh: Kernforschungszentrum Karlsru, 1981.
2. Madelung, O., *Semiconductors: Data Handbook,* Berlin: Springer, 2004.
3. Yu, L.S., Berry, C.J., Drake, R.E., Li, K., Patt, R., Radparvar, M., Whitely, S.R., and Faris, S.M., *IEEE Trans. Magn.,* 1987, vol. 23, p. 1476.
4. Nakagawa, O.N., Nakaya, K., Kurosawa, I., Takada, S., and Hayakawa, H., *Jpn. J. Appl. Phys.,* 1986, vol. 25, p. 70.
5. Hunt, B.D., LeDuc, H.G., Cypher, S.R., and Stern, J.A., *Appl. Phys. Lett.,* 1989, vol. 55, p. 81.
6. Yano, S., Tarutani, Y., Mori, H., Yamada, H., Hirano, M., and Kawabe, U., *IEEE Trans. Magn.*, 1987, vol. 23, p. 1472.
7. Gavaler, J.R., *J. Vac. Sci. Technol.,* 1981, vol. 18, p. 247.
8. Cukauskas, E.J., Carter, W.L., and Qadri, S.B., *J. Appl. Phys.,* 1985, vol. 57, p. 2538.
9. Thakoor, S., Leduc, H.G., Thakoor, A.P., Lambe, J., and Khanna, S.K., *J. Vac. Sci. Technol. A,* 1986, vol. 4, p. 528.
10. Deen, M.J., Landhecr, D., Wade, J.D., Sproule, G.I., and Denoff, M.D., *J. Vac. Sci. Technol. A,* 1988, vol. 6, p. 2299.
11. Hatano, M., Nishino, T., and Kawabe, U., *J. Vac. Sci. Technol. A,* 1988, vol. 6, p. 2381.
12. Talvacchio, J. and Braginski, A.I., *IEEE Trans. Magn.,* 1987, vol. 23, p. 859.
13. Deen, M.J. and Thompson, E.D., *IEEE Trans. Magn.,* 1983, vol. 19, p. 954.
14. Larkins, G.L., Thompson, E.D., Deen, M.J., Burkhart, C.W., and Lando, J.B., *IEEE Trans. Magn.,* 1983, vol. 19, p. 980.
15. Villegier, J.C., Vieux-Rochaz, L., Goniche, M., Renard, P., and Vabre, M., *IEEE Trans. Magn.,* 1985, vol. 21, p. 498.
16. Kosaka, S., Shoji, A., Aoyagi, M., Shinoki, F., Tahara, S., Ohigashi, H., Nagakawa, H., Takada, S., and Hayakawa, H., *IEEE Trans. Magn.,* 1985, vol. 21, p. 102.
17. Shoji, A., Aoyagi, M., Kosaka, S., and Shinoki, F., *IEEE Trans. Magn.,* 1987, vol. 23, p. 1464.
18. LeDuc, H.G., Stern, J.A., Thakoor, S., and Khanna, S.K., *IEEE Trans. Magn.,* 1987, vol. 23, p. 863.
19. Leung, M., Strom, U., Culberston, J.C., Claassen, J.H., Wolf, S.A., and Simon, R.W., *IEEE Trans. Magn.,* 1987, vol. 23, p. 714.
20. Wolf, S.A., Strom, U., Culberston, J.C., and Paget, D., *IEEE Trans. Magn.,* 1985, vol. 21, p. 920.
21. Vachtomin, Yu.B., Finkel, M.L., Antipov, S.V., Voronov, B.M., Smimov, K.V., Kaurova, N.S., Drakinski, V.N., and Gortsman, G.N., *Proc.13th Int. Symposium on Space Temhertz Technology*, Cambridge (MA): Harvard Univ., 2002, p. 259.
22. Hajeniusa, M., Baselmans, J.J.A., Baryshev, A., Gao, J.R., Klapwijk, T.M., Kooi, J.W., Jellema, W., and Yang, Z.Q., *J. Appl. Phys.,* 2006, vol. 100, p. 074507.
23. Khosropanah, P., Gao, J.R., Laauwen, W.M., and Hajenius, M., *Appl. Phys. Lett.,* 2007, vol. 91, p. 221111.
24. Kooi, J.W., Baselmans, J.J.A., Hajenius, M., Gao, J.R., Klapwijk, T.M., Dieleman, P., Baryshev, A., and Lange, G., *J. Appl. Phys.,* 2007, vol. 101, p. 044511.
25. Zhang, J., Slysz, W., Verevkin, A., Okunev, O., Chulkova, G., Korneev, A., Lipatov, A., Gol'tsman, G.N., and Sobolewski, R., *IEEE Trans. Appl. Supercond.,* 2003, vol. 13, no. 2, p. 180.
26. Korneev, A., Lipatov, A., Okunev, O., Chulkova, G., Smirnov, K., Gol'tsman, G., Zhang, J., Slysz, W., Verevkin, A., and Sobolewski, R., *Microelectron. Eng.,* 2003, vol. 69, p. 274.
27. Słysz, W., Węgrzecki, M., Bar, J., Grabiec, P., Górska, M., Zwiller, V., Latta, C., Bohi, P., Milostnaya, I., Minaeva, O., Antipov, A., Okunev, O., Korneev, A., Smirnov, K., Voronov, B., Kaurova, N., Gol'tsman, G., Pearlman, A., Cross, A., Komissarov, I., Verevkin, A., and Sobolewski, R., *Appl. Phys. Lett.,* 2006, vol. 88, p. 261113.

28. Gol'tsman, G., Okunev, O., Chulkova, G., Lipatov, A., Dzardanov, A., Smirnov, K., Semenov, A., Voronov, B., Williams, C., and Sobolewski, R., *IEEE Trans. Appl. Supercond.,* 2001, vol. 11, no. 1, p. 574.
29. Kitaygorsky, J., Zhang, J., Verevkin, A., Sergeev, A., Korneev, A., Matvienko, V., Kouminov, P., Smirnov, K., Voronov, B., Gol'tsman, G., and Sobolewski, R., *IEEE Trans. Appl. Supercond.,* 2005, vol. 15, no. 2, p. 545.
30. Kitaygorsky, J., Komissarov, I., Jukna, A., Pan, D., Minaeva, O., Kaurova, N., Divochiy, A., Korneev, A., Tarkhov, M., Voronov, B., Milostnaya, I., Gol'tsman, G., and Sobolewski, R., *IEEE Trans. Appl. Supercond.,* 2007, vol. 17, no. 2, p. 315.
31. Dietrich, M., May, D., Windte, V., Schauer, M., Schmaderer, F., and Wahl, G., *IEEE Trans. Magn.,* 1987, vol. 23, p. 991.
32. Kampwirth, R.T., Capone, D.W., Gray, K.E., Ho, H., and Chumley, S., *IEEE Trans. Magn.,* 1987, vol. 23, p. 995.
33. Moodera, J.S., Francavilla, T.L., and Wolf, S.A., *IEEE Trans. Magn.,* 1987, vol. 23, p. 1003.
34. Amriou, T., Bouhafs, B., Aourag, H., Khelifa, B., Bresson, S., and Mathieu, C., *Phys. Rev. B: Condens. Matter Mater. Phys.,* 2003, vol. 325, p. 46.
35. Brik, M.G. and Ma, C.G., *Comput. Mater. Sci.,* 2012, vol. 51, p. 380.
36. Rohnke, D.K., Schmatz, D.J., and Hurley, M.D., *Thin Solid Films,* 1984, vol. 118, p. 301.
37. Pogrebnyak, A.D., Yakushchenko, I.V., Sobol', O.V., Beresnev, V.M., Kupchishin, A.I., Bondar, O.V., Lisovenko, M.A., Amekura, H., Kono, K., Oyoshi, K., and Takeda, Y., *Tech. Phys.,* 2015, vol. 60, no. 8, p. 1176.
38. Pogrebnjak, A.D., Yakushchenko, I.V., Bondar, O.V., Sobol', O.V., Beresnev, V.M., Oyoshi, K., Amekura, H., and Takeda, Y., *Phys. Solid State,* 2015, vol. 57, no. 8, p. 1559.
39. Veprek, S., *J. Vac. Sci. Technol. A,* 1999, vol. 17, p. 2401.
40. Veprek, S. and Veprek-Heijman, M.J.G., *Surf. Coat. Technol.,* 2008, vol. 202, p. 5063.
41. Diserens, M., Patscheider, J., and Levy, F., *Surf. Coat. Technol.,* 1998, vols. 108–109, p. 241.
42. Pogrebnjak, A.D., Yakushchenko, I.V., Bagdasaryan, A.A., Bondar, O.V., Krause-Rehberg, R., Abadias, G., Chartier, P., Oyoshi, K., Takeda, Y., Beresnev, V.M., and Sobol, O.V., *Mater. Chem. Phys.,* 2014, vol. 147, no. 3, p. 1079.
43. Pogrebnjak, A.D., Bagdasaryan, A.A., Yakushchenko, I.V., and Beresnev, V.M., *Russ. Chem. Rev.,* 2014, vol. 83, no. 11, p. 1027.
44. Pilloud, D., Pierson, J.F., Marques, A.P., and Cavaleiro, A., *Surf. Coat. Technol.,* 2004, vols. 180–181, p. 352.
45. Bouzakis, K.D., Skordaris, G., Gerardis, S., Katirtzoglou, G., Makrimallakis, S., Pappa, M., Lill, E., and Saoubi, R.M., *Surf. Coat. Technol.,* 2009, vol. 204, p. 1061.
46. Abadias, G., *Surf. Coat. Technol.,* 2008, vol. 202, p. 2223.
47. Holec, D., Friak, M., Neugebauer, J., and Mayrhofer, P.H., *Phys. Rev. B: Condens. Matter Mater. Phys.,* 2012, vol. 85, p. 064101.
48. Pogrebnjak, A.D. and Beresnev, V.M., *Nanocoatings Nanosystems Nanotechnology,* New-York: Bentham Science Publ., 2012.
49. Pogrebnjak, A.D., Bondar, O.V., Abadias, G., Ivashchenko, V.I., Sobol, O.V., Jurga, S., and Coy, E., Ceram. Int., 2016, vol. 42, no. 10, p. 11743.
50. Pogrebnjak, A.D., Eyidi, D., Abadias, G., Bondar, O.V., Beresnev, V.M., and Sobol, O.V., *Int. J. Refract. Met. Hard Mater.,* 2015, vol. 48, p. 222.
51. Boxman, R.L., Zhytomirsky, V.N., Grimberg, I., Rapoport, L., Goldsmith, S., and Weiss, B.Z., *Surf. Coat. Technol.,* 2000, vol. 125, nos. 1–3, p. 257.
52. Veprek, S., *J. Vac. Sci. Technol. A,* 2013, vol. 31, p. 050822.
53. Wolf, S.A., Singer, I.L., Cukauskas, E.J., Francavilla, T.L., and Skelton, E.F., *J. Vac. Sci. Technol.,* 1980, vol. 17, p. 411.
54. Akune, X.T., Sakamoto, N., and Shibuya, Y., *Jpn. J. Appl. Phys.,* 1982, vol. 21, p. 772.
55. Cukauskas, E.J., *J. Appl. Phys.,* 1983, vol. 54, p. 1013.
56. Kobayashi, T., Nakato, Y., and Tsubomura, H., *IEEE Trans. Magn.,* 1987, vol. 23, p. 1007.
57. Koltunowicz, T.N., Zhukowski, P., Bondariev, V., Saad, A., Fedotova, J.A., Fedotov, A.K., Milosavljevic, M., and Kasiuk, J.V., *J. Alloys Compd.,* 2014, vol. 615, no. 1, p. S361.
58. Dong, Y., Liu, Y., Dai, J., and Li, G., *Appl. Surf. Sci.,* 2006, vol. 252, p. 5215.
59. Alfonso, J.E., Buitrago, J., Torres, J., Marco, J.F., and Santos, B., *J. Mater. Sci.,* 2010, vol. 45, no. 20, p. 5528.
60. Martinez, E., Sanjinés, R., Banakh, O., and Lévy, F., *Thin Solid Films,* 2004, vols. 447–448, pp. 332–336.
61. Chang, Ch.L., Lin, Ch.T., Tsai, P.Ch., Ho, W.Yu., and Wang, D.Yu., *Thin Solid Films,* 2008, vol. 516, p. 5324.
62. Sandu, C.S., Medjani, F., and Sanjines, R., *Rev. Adv. Mater. Sci.,* 2007, vol. 15, p. 173.
63. Sandu, C.S., Harada, S., Sanjines, R., and Cavaleiro, A., *Surf. Coat. Technol.,* 2010, vol. 204, p. 1907.
64. Ivashchenko, V.I., Veprek, S., Turchi, P.E.A., and Shevchenko, V.I., *Phys. Rev. B: Condens. Matter Mater. Phys.,* 2012, vol. 85, no. 19, p. 195403.
65. Wen, W., Meng, Q.N., Hu, C.Q., Ana, T., Sua, Y.D., Yua, W.X., and Zheng, W.T., *Surf. Coat. Technol.,* 2009, vol. 203, no. 12, p. 1702.
66. Jeong, J.J. and Lee, C.M., *Appl. Surf. Sci.,* 2003, vol. 214, nos. 1–4, p. 11.
67. Musil, J., *Surf. Coat. Technol.,* 2012, vol. 207, p. 50.
68. Pogrebnjak, A.D., Shpak, A.P., Azarenkov, N.A., and Beresnev, V.M., *Phys.-Usp.,* 2009, vol. 52, no. 1, p. 29.
69. Pogrebnjak, A.D., Beresnev, V.M., Bondar, O.V., Abadias, G., Chartier, P., Postol'nyi, B.A., Andreev, A.A., and Sobol', O.V., *Tech. Phys. Lett.,* 2014, vol. 40, no. 3, p. 215.
70. Pogrebnjak, A.D., Abadias, G., Bondar, O.V., Postolnyi, B.O., Lisovenko, M.O., Kyrychenko, O.V., Andreev, A.A., Beresnev, V.M., Kolesnikov, D.A.,

and Opielak, M., *Acta Phys. Pol. A,* 2014, vol. 125, no. 6, p. 1280.

71. Reid, J.S., Kolawa, E., Ruiz, R.P., and Nicolet, M.A., *Thin Solid Films,* 1993, vol. 236, p. 319.
72. Kim, D.J., Kim, Y.T., and Park, J.W., *J. Appl. Phys.,* 1997, vol. 82, p. 4847.
73. Lee, Y.J., Suh, B.S., Kwom, M.S., and Park, C.O., *J. Appl. Phys.,* 1999, vol. 85, p. 1927.
74. Suh, Y.S., Heuss, G.P., and Misra, V., *Appl. Phys. Lett.,* 2002, vol. 80, p. 1403.
75. Letendu, F., Hugon, M.C., Agius, B., Vickridge, I., Berthier, C., and Lameille, J.M., *Thin Solid Films,* 2006, vol. 513, p. 118.
76. Olowolafe, J.O., Rau, I., Unruh, K.M., Swann, C.P., Jawad, Z.S., and Alford, T., *Thin Solid Films,* 2000, vol. 365, p. 19.
77. Hübner, R., Hecker, M., Mattern, N., Hoffmann, V., Wetzig, K., Heuer, H., Wenzel, Ch., Engelmann, H.J., Gehre, D., and Zschech, E., *Thin Solid Films,* 2006, vol. 500, p. 259.
78. Cabral, C.J., Saenger, K.L., Kotecki, D.E., and Harper, J.M.E., *J. Mater. Res.,* 2000, vol. 15, p. 194.
79. Alén, P., Aaltonen, T., Ritala, M., Leskelä, M., Sajavaara, T., Keinonen, J., Hooker, J.C., and Maes, J.W.J., *Electrochem. Soc.,* 2004, vol. 151, p. G523.
80. Jung, K.M., Jung, M.S., Kim, Y.B., and Choi, K.D., *Thin Solid Films,* 2009, vol. 517, p. 3837.
81. Benkahoul, M., Martinez, E., Karimi, A., Sanjinerѕ, R., and Levy, F., *Surf. Coat. Technol.,* 2004, vol. 180, p. 178.
82. Zhitomirsky, V.N., Grimberg, I., Rapoportc, L., Travitzky, N.A., Boxman, R.L., Goldsmith, S., Raihelc, A., Lapskerc, I., and Weiss, B.Z., *Thin Solid Films,* 1998, vol. 326, p. 134.
83. Oya, G. and Onodera, Yu., *J. Appl. Phys.,* 1976, vol. 47, p. 2833.
84. Sanjinés, R., Benkahoul, M., Papagno, M., Lévy, F., and Music, D., *J. Appl. Phys.,* 2006, vol. 99, p. 044911.
85. Holec, D., Franz, O., Mayrhofer, P.H., and Mitterer, C., *J. Phys. D: Appl. Phys.,* 2010, vol. 43, p. 145403.
86. Ivashchenko, V.I., Skrynskii, P.L., Litvin, O.S., Pogrebnjak, A.D., Rogoz, V.N., Abadias, G., Sobol', O.V., and Kuz'menko, A.P., *Phys. Met. Metallogr.,* 2015, vol. 116, no. 10, p. 1015.
87. Ivashchenko, V.I., Dub, S.N., Scrynskii, P.L., Pogrebnjak, A.D., Sobol', O.V., Tolmacheva, G.N., Rogoz, V.M., and Sinel'chenko, A.K., *J. Superhard Mater.*, 2016, vol. 38, no. 2, p. 103.
88. Sandu, C.S., Benkahoul, M., Parlinska-Wojtan, M., Sanjinés, R., and Lévy, F., *Surf. Coat. Technol.,* 2006, vol. 200, p. 6544.
89. Wen, M., An, T., Du, S., Guo, X., Hu, Ch., Zhang, K., and Zheng, W., *Mater. Sci. Forum,* 2015, vol. 817, p. 137.
90. Thompson, C.V., *Annu. Rev. Mater. Sci.,* 2000, vol. 30, p. 159.
91. Wen, M., Hu, C.Q., Wang, C., An, T., Su, Y. D., Meng, Q.N., and Zheng, W.T., *J. Appl. Phys.,* 2008, vol. 104, p. 023527.
92. Benkahoul, M., Sandu, C.S., Tabet, N., Parlinska-Wojtan, M., Karimi, A., and Levy, F., *Surf. Coat. Technol.,* 2004, vols. 188–189, p. 435.
93. Wang, J., Song, Zh., and Xu, K., *Surf. Coat. Technol.,* 2007, vol. 201, p. 4931.
94. Song, Z.X., Wang, Y., Wang, C.J.F., Liu, C.L., and Xu, K.W., *Surf. Coat. Technol.,* 2007, vol. 201, p. 5412.
95. Han, Z., Hu, X., Tian, J., Li, G., and Mingyuan, G., *Surf. Coat. Technol.,* 2004, vol. 179, p. 188.
96. Kim, S.K., Cha, B.C., and Yoo, J.S., *Surf. Coat. Technol.,* 2004, vols. 177–178, p. 434.
97. Sandu, C.S., Sanjinés, R., Benkahoul, M., Medjani, F., and Lévy, F., *Surf. Coat. Technol.,* 2006, vol. 201, p. 4083.
98. Darlinski, A. and Halbritter, J., *Surf. Interface Anal.,* 1987, vol. 10, p. 223.
99. Fontalvo, G.A., Terziyska, V., and Mitterer, C., *Surf. Coat. Technol.,* 2007, vol. 202, p. 1017.
100. Sanjinés, R., Benkahoul, M., Sandu, C.S., Schmid, P.E., and Lévy, F., *J. Appl. Phys.,* 2005, vol. 98, p. 123511.
101. Patscheider, J., Zehndera, T., and Diserens, M., *Surf. Coat. Technol.,* 2001, vols. 146–147, p. 201.

*Translated by M. Timoshinina*